Bond patterns and charge-order amplitude in quarter-filled charge-transfer solids

R. T. Clay, A. B. Ward, N. Gomes, and S. Mazumdar

Phys. Rev. B **95**, 125114 — Published 10 March 2017

DOI: 10.1103/PhysRevB.95.125114

Bond patterns and charge order amplitude in $\frac{1}{4}$-filled charge-transfer solids

R.T. Clay,[1,*] A.B. Ward,[1] N. Gomes,[2] and S. Mazumdar[2,3]

[1] *Department of Physics and Astronomy and HPC² Center for Computational Sciences, Mississippi State University, Mississippi State MS 39762*

[2] *Department of Physics, University of Arizona Tucson, AZ 85721*

[3] *Department of Chemistry, University of Arizona Tucson, AZ 85721*

Most quasi-one-dimensional (quasi-1D) $\frac{1}{4}$-filled organic charge-transfer solids (CTS) with insulating ground states have two thermodynamic transitions, a high-temperature metal-insulator transition followed by a low-temperature magnetic transition. This sequence of transitions can be understood within the 1D Peierls-extended Hubbard (PEH) model. However, in some quasi-1D CTS both transitions occur simultaneously in a direct metal to spin-gapped insulator transition. In this second class of materials the organic stack bond distortion pattern does not follow the pattern of a second dimerization of a dimer lattice. These materials also display charge ordering of a large amplitude below the transition. Using quantum Monte Carlo methods we show that the same PEH model can be used to understand both classes of materials, however in a parameter region not previously studied. We discuss the relevance of our work to experiments on several $\frac{1}{4}$-filled conductors, focusing in particular on the materials (EDO-TTF)$_2$X and (DMEDO-TTF)$_2$X.

PACS numbers: 71.10.Fd, 71.45.Lr, 74.70.Kn

I. INTRODUCTION

Molecular charge transfer solids (CTS) are widely studied because of their many complex electronic states. Small structural changes can lead to very different electronic behaviors. These effects have been studied extensively in the quasi-one dimensional (quasi-1D) CTS, in particularly for the $\frac{3}{4}$-filled (with density $\rho = 0.5$ holes per molecule) materials (TMTSF)$_2$X and (TMTTF)$_2$X, which become superconducting under the application of pressure[1]. The ground state of a 1D system of electrons with coupled lattice degrees of freedom is an insulating Peierls state. It is often assumed for strongly correlated $\rho = 0.5$ systems that this insulating ground state is reached through two thermodynamic transitions, with bond dimerization or period two charge order (CO) occurring first at the higher metal-insulator (MI) transition, followed by a small amplitude bond alternation between the localized charges or dimers (for a recent review see reference 2). Examples of materials with two transitions are MEM(TCNQ)$_2$ and (TMTTF)$_2$X.

However, in some $\rho = 0.5$ quasi-1D CTS, a *single* transition takes place between the high temperature metallic state and the low temperature spin gapped state. This single transition is accompanied by the opening of both charge and spin gaps. CO amplitudes for this second class of materials are large, with high transition temperatures. One example is (EDO-TTF)$_2$PF$_6$, where the transition temperature is 280 K and the CO amplitude below the transition is approximately 0.9:0.1 [3–5]. It has been assumed that the simplest model incorporating electron-electron (e-e) and electron-phonon (e-p) interactions, the Peierls-extended Hubbard model (see Section II A), cannot account for this large CO amplitude[4,6]. It has been suggested that additional interactions, such as molecular bending[7] or electronic polarization effects[6] are therefore driving the transition. A similar material is (DMEDO-TTF)$_2$X, X = ClO_4 and BF_4, where there is also a single transition. It has been proposed that anions drive the transition[8]. The CO amplitude is currently unknown.

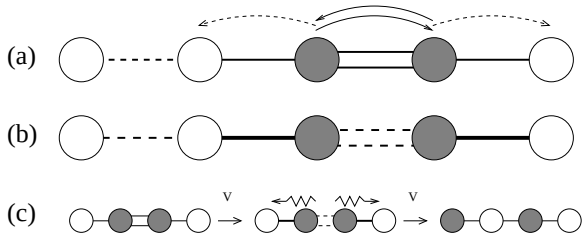

FIG. 1: Bond distortion patterns coexisting with $\cdots 1100 \cdots$ CO in the $\frac{1}{4}$-filled band. Filled (unfilled) circles indicate molecules with charge density $0.5 + \delta$ ($0.5 - \delta$). (a) BCDW2 with bond distortion pattern Strong-Medium-Weak-Medium (SMWM). The double line indicates a stronger bond (S) than a single line (M), and solid lines indicate bonds stronger than dashed lines (W). The arrows indicate charge transfer paths which influence the relative strength of the 1–1 and 1–0 bonds (see Section II B). (b) BCDW1 with pattern Strong-Weak-Strong-Weak′ (SWSW′). The single (S) bond is strongest, followed by double-dashed (W′) and single-dashed (W). (c) Schematic evolution with increasing nearest-neighbor Coulomb repulsion V from BCDW2 → BCDW1 → $4k_F$ CO. For moderate V, Coulomb repulsion of the neighboring charge-rich sites *strengthens* the BCDW1 bond distortion (see text).

The goal of the present work is to show that bond distorted states with both small and large CO amplitudes can be understood *within the same one-dimensional fundamental theoretical model,* albeit within different parameter regions. Molecular bending[7] and cation-anion interactions[8] act *cooperatively* with the underlying bond distortion of the organic stacks. Through a systematic numerical study, we show that with increasing e-e interaction strength, a crossover occurs between two different

bond-charge-density waves (BCDWs) which we will label BCDW1 and BCDW2 (see Fig. 1). BCDW1 (Fig. 1(b)) has been widely studied and is intuitively understood as a second dimerization of a dimer lattice. The BCDW2 bond distortion pattern, however, (Fig. 1(a)) *does not* fit the pattern of dimerization of a dimer lattice. We show that the BCDW2 is characterized by much larger charge disproportionation amplitude than BCDW1.

The outline of the paper is as follows: in Section II A we define the model and theoretical quantities, followed by calculations in the limit of zero e-p interactions in II B, and BCDW order parameters in II C. In Section III we compare our results with experimental studies of several materials.

II. RESULTS

A. Theoretical Framework

A well established minimal model for the 1D CTS is the 1D Peierls-extended Hubbard model,

$$\begin{aligned} H &= -\sum_{i\sigma}[t-\alpha\Delta_i](c^\dagger_{i+1,\sigma}c_{i,\sigma}+H.c.)+\frac{1}{2}K_1\sum_i\Delta_i^2 \\ &+ g\sum_i\nu_i n_i+\frac{1}{2}K_2\sum_i\nu_i^2 \\ &+ U\sum_i n_{i,\uparrow}n_{i,\downarrow}+V\sum_i n_{i+1}n_i. \end{aligned} \quad (1)$$

In Eq. 1, $c^\dagger_{i,\sigma}$ ($c_{i,\sigma}$) creates (annihilates) an electron of spin σ on site i, $n_{i,\sigma}$=$c^\dagger_{i,\sigma}c_{i,\sigma}$, and n_i=$n_{i,\uparrow}+n_{i,\downarrow}$. Δ_i is the deviation of the bond between sites i and $i+1$ from its equilibrium length and α is the inter-site e-p coupling with spring constant K_1. Intra-molecular distortions on each molecule are parameterized by the phonon coordinate ν_i; g is the intra-site e-p coupling with K_2 its corresponding spring constant. U and V are the onsite and nearest-neighbor Coulomb interactions respectively. We give energies in units of t.

At $\frac{1}{4}$-filling ($\rho=0.5$), charge- and bond-ordering at $2k_F$ (period four) or $4k_F$ (period two) dominate. The occurrence of $4k_F$ CO requires $V>V_c$, where the critical value[9] $V_c=2$ in the limit $U\to\infty$ but is larger than 2 for finite U (see Fig. 3). In applying Eq. 1 to the 1D CTS, it is also expected that $V<\frac{U}{2}$, based on comparison to $\rho=1$ 1D CTS[10]. Here we restrict our analysis to (U,V) with $V<V_c$ and $V<\frac{U}{2}$. A general form for Δ_j can be written as[11]

$$\Delta_j=\Delta_0[a_2\cos(2k_Fj-\phi_2)+a_4\cos(4k_Fj-\phi_4)], \quad (2)$$

where Δ_0 is the overall amplitude of the bond distortion, a_2 and a_4 are the amplitude of $2k_F$ and $4k_F$ components respectively, and ϕ_2 and ϕ_4 their phases.

For moderate U and V, the two bond distortion patterns that occur[11] are shown in Fig. 1. In both the charge density follows the pattern $\cdots1100\cdots$, where 1 (0) indicates a molecule with charge density 0.5+δ (0.5-δ). In BCDW2 (Fig. 1(a)) the strongest bond is between the two large charge densities, and the hopping integrals follow the pattern strong-medium-weak-medium (SMWM). In BCDW1 (Fig. 1(b)), the pattern of hopping integrals in the ground state is instead strong-weak-strong-weak′ (SWSW′) in Fig. 1(b)), where the W bond is slightly weaker than the W′ bond.

Prior theoretical work[2] has focused almost entirely on the competition between BCDW1 and the $4k_F$ CO, and only large U and V near V_c has been studied. In this region the amplitude of the $2k_F$ CO is weak[12–15]. As we will show in the next sections, this is not always the case– for moderate U and V in combination with strong e-p coupling, the CO amplitude can be quite large, *provided the bond pattern is that of BCDW2.*

B. Effect of U and V on bond distortion pattern

Before presenting our numerical results we show how the existence of BCDW2 at small (U,V) and a crossover to BCDW1 at larger (U,V) are to be anticipated, from configuration space based physical arguments. The arrows in Fig. 1(a) indicate possible charge transfers within the $\cdots1100\cdots$ CO configuration. The expectation value of the charge transfer in the ground state wavefunction is the bond order, the strength of the bond. As indicated in the figure, there are two possible charge transfers across the 1–1 bond, giving the configurations $\cdots2000\cdots$ and $\cdots0200\cdots$ In contrast charge transfer across the 1–0 bond occurs only in one direction, and there is no charge transfer across the 0–0 bond. Thus the 0–0 bond is weaker than either of the other two bonds. At weak U the penalty for double occupancy is small, and two possible charge transfers across the 1–1 bond is therefore enough to make this bond stronger than the 1–0 bond. As U increases, the larger penalty for double occupancy outweighs the larger number of charge transfers, and the reverse becomes true. The effect of V can be understood within the same physical picture, as is indicated in Fig. 1(c). At the extreme left is the BCDW2 configuration with the 1–1 bond the strongest. As V is slowly increased from 0, initially it simply pushes the charge-rich sites further apart, making the 1–1 bond weaker and the 1–0 bonds stronger, without actually destroying the basic $\cdots1100\cdots$ arrangement. This suggests that there exists a region in phase space where for each U there is a range of V where the V actually enhances the $\cdots1100\cdots$ BCDW1. This occurs until $V>V_c$, where the transition to the $4k_F$ CO occurs.

The above is for the spin singlet ground state only. As the temperature is raised, the free energy is dominated more and more by high spin states with greater multiplicities. Note that in the ferromagnetic configuration there can be no charge transfer across the 1–1 bond, and it becomes equivalent to the 0–0 bond. There then ex-

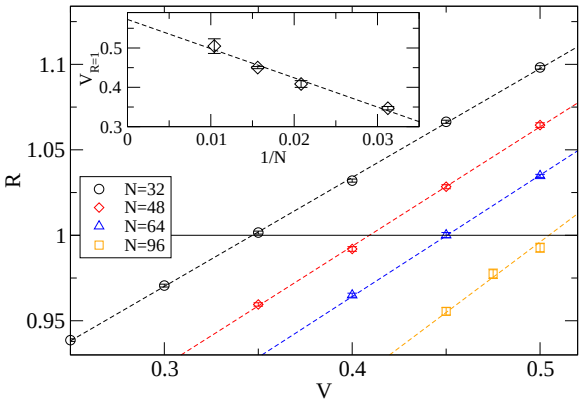

FIG. 2: (color online) Crossover between BCDW1 and BCDW2 in the limit of zero e-p interactions (a) $R = \chi_B(4k_F)/\chi_B(2k_F)$ as a function of V with $U = 6.25$. Circles, diamonds, triangles, and squares are for 32, 48, 64, and 96 site chains, respectively. Systems with R below the horizontal line $R = 1$ will distort in the BCDW2 bond pattern. The inset shows the finite-size scaling of $V_{R=1}$, the V for which $R = 1$.

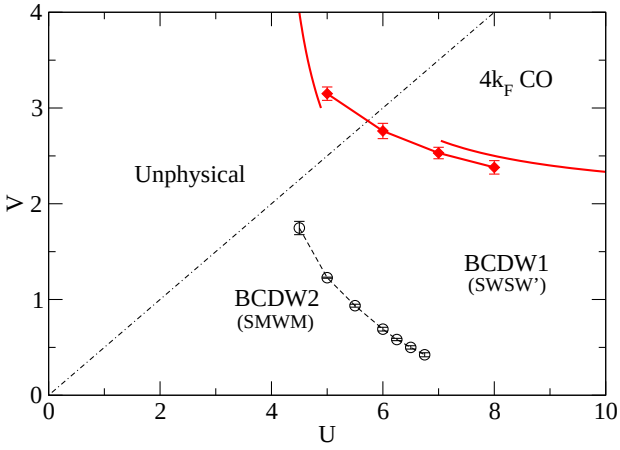

FIG. 3: (color online) Zero temperature phase diagram of Eq. 1 in the limit of 0^+ e-p interactions at $\frac{1}{4}$ filling. Open points are the crossover boundary between BCDW2 and BCDW1 regions. Solid diamonds and solid lines mark the boundary to the $4k_F$ CO region (see Ref. 13). The $V = \frac{U}{2}$ line indicates the region of physical relevance for organic CTS.

ists a temperature where the high spin states contribute more than the singlet state to the free energy, and the BCDW1 transforms to the bond-dimerized state. Since large U raises the energy of the spin singlet state relative to the high spin states, bringing them closer, it follows that the larger the U, the greater is the tendency to the $4k_F$ bond dimerization, provided $V < V_c$.

The tendency to bond distortion at wavevector q is measured by the bond susceptibility[16], $\chi_B(q)$, defined as

$$\chi_B(q) = \frac{1}{N}\sum_{j,l}\int_0^\beta e^{iq(j-l)}\langle \tilde{B}_j(\tau)\tilde{B}_l(0)\rangle d\tau. \qquad (3)$$

In Eq. 3, $\tilde{B}_j(\tau) = e^{-\tau H}\tilde{B}_j e^{\tau H}$ where $\tilde{B}_j = B_j - \langle B\rangle$ and $B_j = \frac{1}{2}\sum_\sigma (c^\dagger_{j+1,\sigma}c_{j,\sigma} + H.c.)$. β is the inverse temperature and N the number of sites. The crossover from BCDW2 to BCDW1 occurs at a specific ratio of a_4 to a_2 in Eq. 2 and may therefore in the limit of 0^+ e-p phonon coupling be determined by comparing $\chi_B(2k_F)$ and $\chi_B(4k_F)$.

In Eq. 2 the phase angles for both BCDW states are[11] $\phi_2 = \frac{\pi}{2}$ and $\phi_4 = 0$. While BCDW2 is nearly a pure $2k_F$ bond distortion, BCDW1 requires a significant $4k_F$ component. The minimum a_4 in Eq. 2 for the BCDW1 pattern occurs when the 'S' and 'W'' bonds are of equal strength. From this one can derive the condition that $a_4/a_2 > \frac{1}{2}$ for BCDW1[11,17]. Further assuming the normalization $a_2 + a_4 = 1$, this implies $a_4 > \frac{1}{3}$ for BCDW1.

The discrete Fourier transform of $\Delta_j\Delta_l$ with respect to $(j-l)$ is $\Delta_0^2 a_2^2 N/4$ at $q = \pi/2$ and $\Delta_0^2 a_4^2 N$ at $q = \pi$. Therefore, in the limit of 0^+ e-p coupling $\chi_B(4k_F)/\chi_B(2k_F) = 4a_4^2/a_2^2$ and the BCDW1 pattern will occur when $\chi_B(4k_F)/\chi_B(2k_F) > 1$. The bond distortion changes smoothly between BCDW1 and BCDW2 without any discontinuity in the bond distortion or other observables. In the purely 1D model of Eq. 1 this is a crossover and not a quantum phase transition. However, we expect that in a full 3D model of the actual materials, the BCDW1 and BCDW2 regions may correspond to thermodynamically distinct phases (see Section III).

We use the Stochastic Series Expansion (SSE) quantum Monte Carlo method with directed loop updates to calculate $\chi_B(q)$[18,19]. SSE is free from the Fermion sign problem in 1D and provides exact (within statistical errors) results at finite temperatures. We calculated the ratio $R = \chi_B(4k_F)/\chi_B(2k_F)$ for periodic systems of $N =$ 32, 48, 64, and 96 sites with an inverse temperature of $\beta = 4N$, which is a low enough temperature to give essentially ground state results. $\chi_B(4k_F)$ increases with increasing V; for each system size, the V where $R = 1$ was determined keeping U fixed, as shown in Fig. 2. We then performed a finite-size scaling using a linear fit of the transition points to $1/N$; a typical fit is shown in the inset of Fig. 2. Fig. 3 shows the location of the crossover in the (U,V) plane. In Fig. 3 we also include the boundary for the $4k_F$ CO phase[2,9] from Reference 13, which are determined from the condition that the Luttinger Liquid exponent $K_\rho > \frac{1}{3}$, indicating dominant $4k_F$ charge fluctuations[20]. The solid lines in Fig. 3 are the result of second order perturbation theory about the $U \to \infty$ and $V \to \infty$ limits[9,21]. In the rest of the paper we focus on the BCDW1 and BCDW2 charge and bond order amplitudes.

C. Charge order amplitude

We define the amplitude of the CO as $\Delta n = \langle n_{large}\rangle$ - $\langle n_{small}\rangle$, where n_{large} and n_{small} are the charge densities on the charge-rich and charge-poor molecules. Δn

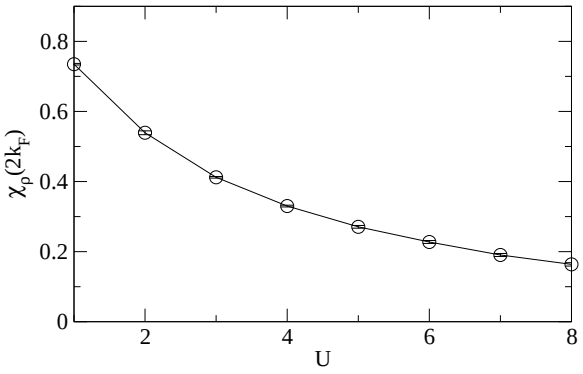

FIG. 4: $2k_F$ charge susceptibility as a function of U for a 48 site chain with $V = U/4$, $\alpha = g = 0$, and inverse temperature $\beta = 192$.

is of great experimental interest and can be measured optically[22] and by NMR[23]. Theoretically, Δn is difficult to predict from Eq. 1, as it depends on the precise values of the e-p coupling constants α and g which are difficult to estimate.

In the limit of $\alpha = g = 0$, the $2k_F$ charge susceptibility ($\chi_\rho(q)$) is defined as in Eq. 3 with $\tilde{B}_j$ replaced by $n_j - \langle n \rangle$) decreases[24] with increasing U, implying that Δn is smaller in BCDW1 compared to BCDW2. In Fig. 4 we show $\chi_\rho(2k_F)$ as a function of U calculated along the line $V = U/4$. Fig. 4 shows that differences in e-e correlation alone can account for approximately a factor of four in the magnitude of Δn between the most weakly-correlated CTS salts compared to those with strong e-e correlations, assuming equal e-p coupling strengths.

To calculate Δn in Eq. 1 with e-p interactions, we use a zero temperature variational quantum Monte Carlo using a matrix-product state basis (MPS-QMC)[25,26]. Matrix-product states are extremely efficient for representing the wavefunctions of interacting 1D quantum systems. The MPS-QMC method variationally optimizes the MPS matrices from random starting values using stochastic optimization[25]. One advantage of MPS-QMC is that periodic systems can be easily treated. Further details of the method are given in Reference 26. To handle the e-p degrees of freedom self-consistently, Δ_i in Eq. 1 is taken to be of the form of Eq. 2 with fixed ϕ_2 and ϕ_4. Fixing the bond distortion to this form is reasonable for U and V not too close to the $4k_F$ CO region. ν_i are taken with a constant magnitude ν and a fixed pattern $\cdots--++\cdots$ giving $\cdots 1100 \cdots$ CO. Self-consistency equations for Δ_0, a_4, and ν are determined from[13]

$$\frac{\partial\langle H\rangle}{\partial\Delta_0} = 0, \qquad \frac{\partial\langle H\rangle}{\partial a_4} = 0, \qquad \frac{\partial\langle H\rangle}{\partial\nu} = 0. \qquad (4)$$

For the results presented here, matrix dimensions D of up to 32 were used[26]. We used chain lengths from 16 up to 64 sites and finite-size scaled the results using linear extrapolation in $1/N$; Fig. 5(a) shows typical finite-size extrapolations for the case $\alpha = 1.2$ and $g = 0$.

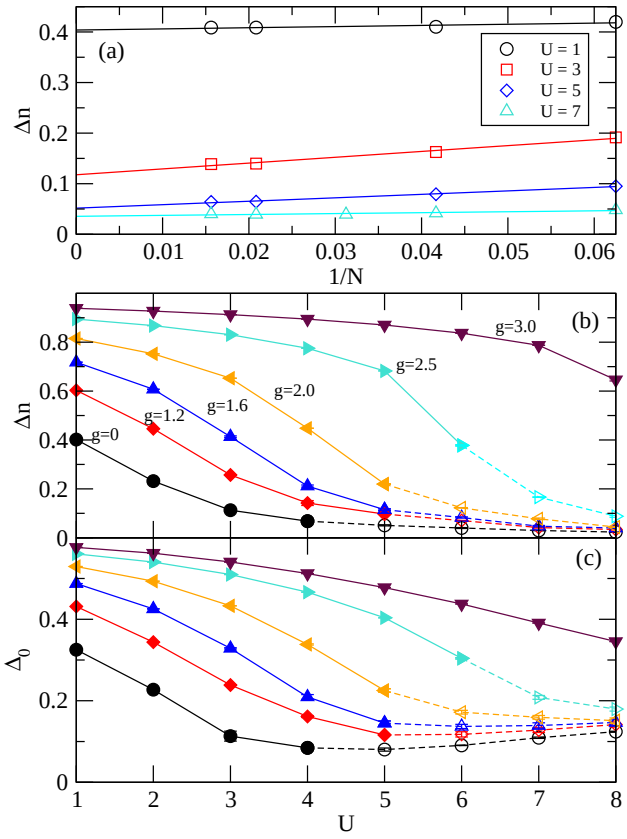

FIG. 5: (color online) Results of self-consistent MPS calculations (see text). For all panels $V = U/4$. (a) Finite size scaling of the charge order amplitude Δn versus inverse chain length with $\alpha = 1.2$ and $g = 0$. Lines are linear fits. (b) Finite-size scaled Δn as a function of U and g, with $\alpha = 1.2$. (c) The overall amplitude of the bond distortion (see Eq. 2) for the parameters of (b). In both (b) and (c) the filled (open) points correspond to BCDW2 (BCDW1) and lines are guides to the eye.

The intra-site e-p interaction couples directly to the charge density and affects Δn strongly. We first choose a fixed α and vary g in Eq. 1. Figs. 5(b) and (c) summarize the results of these calculations. For $g \lesssim 2$, Δn versus U has a very similar functional shape as the $2k_F$ charge susceptibility in Fig. 4, confirming that e-e interactions strongly affect Δn. The maximum Δn for $g = 0$ is ≈ 0.4 at small U. As seen in Figs. 5(b) and (c), the bond pattern switches to BCDW1 at $U \approx 5$, which is consistent with Fig. 3.

As shown in Fig. 5(b), in BCDW2, Δn is strongly enhanced by g up to nearly complete charge transfers of $\Delta n \approx 0.9$. BCDW1 however is characterized by small Δn for all g, which for most parameters choices is $\lesssim 0.1$. While in general weaker e-e correlations coincide with larger Δn, Fig. 5 shows that as g increases the crossover between BCDW2 and BCDW1 moves to larger U and V (i.e. the BCDW2/BCDW1 line in Fig. 3 moves towards the $4k_F$ CO phase with increasing g). Fig. 5 also shows that large enough g suppresses BCDW1 altogether. It is

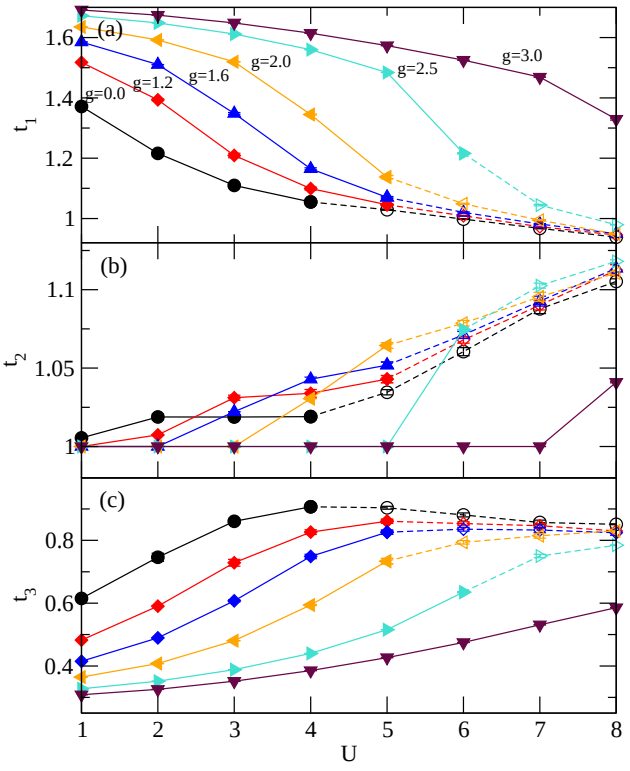

FIG. 6: (color online) Hopping integrals for the same parameters as Fig. 5.

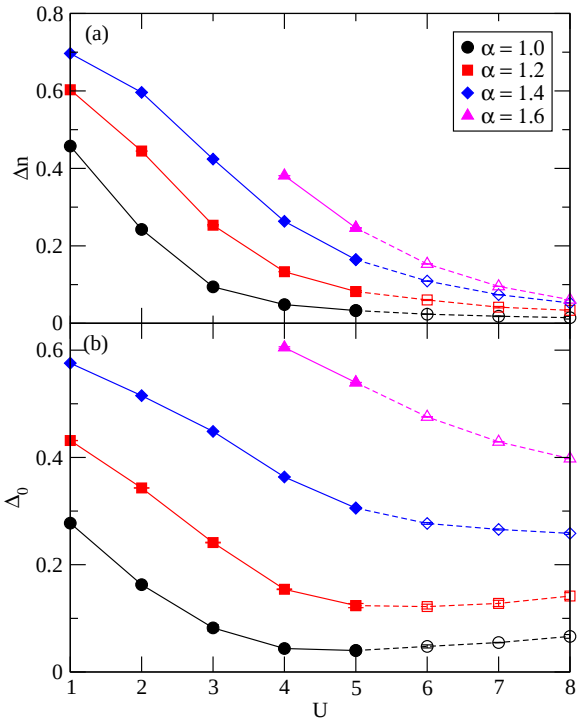

FIG. 7: (color online) (a) Finite-size scaled Δn as a function of U and α with $g = 1.2$. (c) The overall amplitude of the bond distortion (see Fig. 5(c)).

also possible that large g in combination with U and V near the $4k_F$ CO phase results in $\cdots 1010 \cdots$ CO[13].

Importantly, at large U, the strength of the bond distortion behaves differently from Δn. While the amplitude of the $\cdots 1100 \cdots$ CO decreases continuously as the strength of e-e interactions increases, Fig. 5(c) shows that the BCDW1 the overall bond distortion strength Δ_0 *increases* with the e-e interaction strength for $U \gtrsim 5$ and $g \lesssim 2$ (see Section II B).

In the interest of comparing with experimental data, in Fig. 6 we show the actual hopping integrals. Corresponding to the charge order pattern $\cdots 1100 \cdots$ we define the '1–1' bond as t_1, the '1–0' and '0–1' bonds as t_2 and the '0–0' bond as t_3, respectively. In the BCDW2 pattern SMWM, t_1 is the strong S bond, t_2 the M bond, and t_3 the W bond. In the BCDW1 pattern SWSW′, t_1 is the W′ bond, t_2 the S bond, and t_3 the W bond. The decrease in t_1 in Fig. 6(a) and the simultaneous increase in t_2 in Fig. 6(b) are signatures of the crossover from BCDW2 to BCDW1 with increasing U.

In Fig. 7 we show the result of varying the inter-site e-p coupling α. Unlike g, α can only be varied over a relatively small range. For finite systems a minimum value of α is required for the lattice distortion to occur. For *too* large α the linear e-p coupling in Eq. 1 leads to a negative bond order for the weakest bonds indicating a failure of the linear coupling assumption (this occurs for $\alpha = 1.6$ and $U < 4$ in Fig. 7)[13]. Fig. 7 shows that varying α has an effect similar to varying g: stronger e-p coupling can enhance Δn strongly in the BCDW2 region, and at the same time moves the system towards BCDW2. Fig. 8 further shows the hopping integrals in this case. Increasing α can strongly increase the amplitude of the bond distortion in BCDW1 (see strong increase in Fig. 8(b)), even as Δn remains small (see Fig. 7(a)).

Summarizing our data, in BCDW2 Δn can have any value up to ≈ 0.9 depending on the e-e and e-p interaction strengths. However, regardless of the choice of e-e interactions and e-p coupling strength, Δn for BCDW1 is always small—the maximum in all of our calculations was $\Delta n \approx 0.2$. More typically Δn in BCDW1 is in the range $0.05 \sim 0.1$.

III. DISCUSSION

Within Eq. 1 BCDW1 and BCDW2 are not distinct thermodynamic phases and the boundary between them a crossover. We have however, showed that order parameters of BCDW2, both the bond distortion and CO amplitude, are significantly larger than in BCDW1. Two transitions are expected for BCDW1 because of the large separation in energy scales between the high temperature MI transition (involving bond dimerization or period two CO) and the small amplitude distortion below the insulator-insulator transition. This separation however, is likely to break down for the large amplitude BCDW2

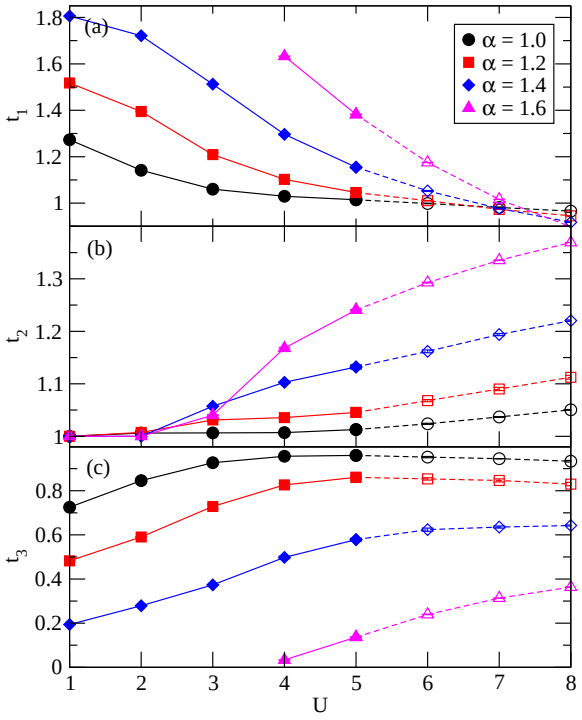

FIG. 8: (color online) Hopping integrals for the same parameters as Fig. 7.

bond and charge distortion. Note that dimerization of the dimerization requires that the bond dimerization at the MI transition that creates the charge gap is necessarily larger than the second dimerization driven by spin interactions at lower temperature. Since in the BCDW2, the two equivalent 1–0 bonds are weaker than the 1–1 bond, it follows that this structure cannot arise from dimerization of dimerization. Put alternatively, spin excitations involve the stronger 1–1 bond, which implies that the energy separation between the charge and spin gap will tend to vanish. Hence, from the pattern of the distortion itself, there is very likely a single transition in systems exhibiting BCDW2.

A. BCDW2

We first discuss two families of CTS whose low-temperature insulating states show the BCDW2 bond pattern, $(EDO\text{-}TTF)_2X$ (X = PF_6 and AsF_6) and $(DMEDO\text{-}TTF)_2X$ (X = ClO_4 and BF_4). In each of these materials the MI transition has been attributed to different effects, such as e-p and coupled molecular bending[7] or electrical potential bias originating from long-range Coulomb interactions[6] in $(EDO\text{-}TTF)_2X$, and anion ordering in $(DMEDO\text{-}TTF)_2X$[8]. We argue that these are instead *cooperative* effects[3] (see below). The features common to BCDW2 are clearly seen by comparing $(EDO\text{-}TTF)_2X$ and $(DMEDO\text{-}TTF)_2X$, which show the same molecular stack distortion but somewhat different secondary effects.

$(EDO\text{-}TTF)_2X$: In $(EDO\text{-}TTF)_2X$ the MI transition is first order and occurs at 280 K and 268 K for X=PF_6 and AsF_6, respectively[3]. A third salt, X=ClO_4, has an even higher transition temperature, greater than 337 K[27]. In $(EDO\text{-}TTF)_2PF_6$ the experimentally determined CO amplitude is rather large, with estimates of Δn from optical measurements of 0.92 (T=6 K)[4] or from X-ray measurements of 0.6 (T =260 K)[5]. Above the transition, the molecular overlaps along the EDO-TTF stacks are nearly uniform with only a slight dimerization[3]. Below the transition the overlap integrals follow the predicted pattern SMWM[3].

Several observations indicate that intra-site e-p interactions are strongly involved in the MI transition. At the transition, the EDO-TTF molecules bend significantly[3], with the dihedral angles between the center and terminal groups of the molecules changing by more than 5°. The degree of bending depends on the charge density on each molecule, with charge-rich molecules becoming flatter[3,4]. The transfer integral between flatter molecules is enhanced, strengthening the '1–1' bond and cooperatively enhancing the bond distortion[3,4]. The position of the anions also shift, with a periodic modulation that matches that of the EDO-TTF stacks[3]. Optical studies of $(EDO\text{-}TTF)_2X$ have suggested that the observed high sensitivity to photoexcitation is likely due to strong electron-lattice coupling[28].

$(DMEDO\text{-}TTF)_2X$: Here the MI transition is at 190 K and 210 K for X=ClO_4 and BF_4, respectively[8,29]. Above the MI transition the organic molecules are stacked uniformly, and like $(EDO\text{-}TTF)_2X$ the low temperature overlap integrals are in the SMWM pattern[8]. Simultaneously with the stack distortion, the anion positions shift, moving closer (further) towards molecules with large (smaller) hole density. The authors of Reference 8 ascribe the MI transition to this anion shift, in which the ClO_4 group moves towards and away from charge-rich and charge-poor molecules. The electrostatic potential of the anions enhances Δn of the organic stack, which further strengths the strong 'S' bond. Shortening the 'S' bond (bond b_1 in Fig. 7(c) of Reference 8) moves the hole-rich molecules closer to the anions. This feedback loop between the anions and the bond distortion will cooperatively strengthen BCDW2. A similar anion shift occurs[5] in $(EDO\text{-}TTF)_2X$. While Δn estimated from carbon-carbon bond lengths appears to be small this method of estimating CO amplitude however has large errors[8]. We predict that more direct measurements for example using optical techniques will find large Δn in this material.

To obtain the large Δn found in $(EDO\text{-}TTF)_2X$, our results of Section II show that large intra-site e-p coupling (and moderate or small e-e correlations) are required. The strong coupling to molecular bending in $(EDO\text{-}TTF)_2X$ shows that intra-molecular modes are coupled strongly in this case. Large Δn would also make the contribution from longer-range Coulomb interactions signif-

icant, which could further enhance 1100 pattern CO[30].

B. BCDW1

As the thermodynamics of materials with the BCDW1 have been extensively studied[10,12–15], we will not discuss them in detail here. The BCDW1 state can be visualized as a second dimerization of a dimer lattice. Within the full three-dimensional crystal two thermodynamic transitions are expected[10,13–15]. What the present calculations show is that in the ground state, the expected CO amplitude in BCDW1 is quite small and may be difficult to detect experimentally. This should also be taken into consideration in searches for CO in two dimensional CTS[31]. To detect the presence of BCDW1, it may be easier to focus on the pattern of bond distortion rather than the amount of CO.

IV. ACKNOWLEDGMENTS

This work was supported by the Department of Energy grant DE-FG02-06ER46315. Part of the calculations were performed using resources of the National Energy Research Scientific Computing Center (NERSC), which is supported by the Office of Science of the U.S. Department of Energy under Contract No. DE-AC02-05CH11231.

* Electronic address: r.t.clay@msstate.edu

[1] T. Ishiguro, K. Yamaji, and G. Saito, *Organic Superconductors* (Springer-Verlag, New York, 1998).
[2] H. Yoshioka, Y. Otsuka, and H. Seo, Crystals **2**, 996 (2012).
[3] A. Ota, H. Yamochi, and G. Saito, J. Mater. Chem. **12**, 2600 (2002).
[4] O. Drozdova, K. Yakushi, K. Yamamoto, A. Ota, H. Yamochi, G. Saito, H. Tashiro, and D. B. Tanner, Phys. Rev. B **70**, 075107 (2004).
[5] S. Aoyagi, K. Kato, A. Ota, H. Yamochi, G. Saito, H. Suematsu, M. Sakata, and M. Takata, Angew. Chem. Int. Ed. **43**, 3670 (2004).
[6] K. Iwano and Y. Shimoi, Phys. Rev. B **77**, 075120 (2008).
[7] M. Tsuchiizu and Y. Suzumura, Phys. Rev. B **77**, 195128 (2008).
[8] S. Kumeta, T. Kawamoto, T. Shirahata, Y. Misaki, and T. Mori, J. Phys. Soc. Jpn. **85**, 094701 (2016).
[9] F. Mila and X. Zotos, Europhys. Lett. **24**, 133 (1993).
[10] R. T. Clay, R. P. Hardikar, and S. Mazumdar, Phys. Rev. B **76**, 205118 (2007).
[11] K. C. Ung, S. Mazumdar, and D. Toussaint, Phys. Rev. Lett. **73**, 2603 (1994).
[12] S. Mazumdar, R. T. Clay, and D. K. Campbell, Phys. Rev. B **62**, 13400 (2000).
[13] R. T. Clay, S. Mazumdar, and D. K. Campbell, Phys. Rev. B **67**, 115121 (2003).
[14] H. Seo, Y. Motome, and T. Kato, J. Phys. Soc. Jpn. **76**, 013707 (2007).
[15] Y. Otsuka, H. Seo, Y. Motome, and T. Kato, J. Phys. Soc. Jpn. **77**, 113705 (2008).
[16] J. E. Hirsch and D. J. Scalapino, Phys. Rev. B **29**, 5554 (1984).
[17] In References 11 and 26 the bond distortion pattern is written in terms of u_j, the displacement of the jth site from equilibrium, with $2k_F$ and $4k_F$ weights r_2 and r_4. In the present notation $\Delta_j = u_{j+1} - u_j$. The ratio of $4k_F$ to $2k_F$ components required for the BCDW2 phase was quoted incorrectly in these references–rather than 0.41, $r_4/r_2 > \frac{\sqrt{2}}{4+\sqrt{2}} = 0.26$ for the BCDW2 pattern.
[18] A. W. Sandvik, J. Phys. A **25**, 3667 (1992).
[19] O. F. Syljuasen and A. W. Sandvik, Phys. Rev. E **66**, 046701 (2002).
[20] J. Voit, Rep. Prog. Phys. **58**, 977 (1995).
[21] H. Q. Lin, D. K. Campbell, and R. T. Clay, Chinese J. Phys. **11**, 1 (2000).
[22] M. Dressel, M. Dumm, T. Knoblauch, and M. Masino, Crystals **2**, 528 (2012).
[23] F. Zamborszky, W. Yu, W. Raas, S. E. Brown, B. Alavi, C. A. Merlic, and A. Baur, Phys. Rev. B **66**, 081103 (2002).
[24] J. E. Hirsch and D. J. Scalapino, Phys. Rev. B **27**, 7169 (1983).
[25] A. W. Sandvik, Phys. Rev. Lett. **101**, 140603 (2008).
[26] R. T. Clay, J. P. Song, S. Dayal, and S. Mazumdar, J. Phys. Soc. Jpn. **81**, 074707 (2012).
[27] A. Ota, H. Yamochi, and G. Saito, Synth. Metals **133-134**, 463 (2003).
[28] M. Chollet, L. Guerin, N. Uchida, S. Fukaya, H. Shimoda, T. Ishikawa, K. Matsuda, T. Hasegawa, A. Ota, H. Yamochi, et al., Science **307**, 86 (2005).
[29] J. M. Fabre, S. Chakroune, A. Javidan, L. Zanik, L. Ouahab, S. Golhen, and P. Delhaes, Synth. Metals **70**, 1127 (1995).
[30] J. Hubbard, Phys. Rev. B **17**, 494 (1978).
[31] K. Sedlmeier, S. Elsässer, D. Neubauer, R. Beyer, D. Wu, T. Ivek, S. Tomic, J. A. Schlueter, and M. Dressel, Phys. Rev. B **86**, 245103 (2012).